

Chapter 8

Unsteady Transition Phenomena at the Leading Edge of Compressor Blades

Unsteady flow arising from interactions between adjacent blade rows in axial turbomachinery usually results in multi-moded transition on blade surfaces. This was discussed in review papers by Mayle [111] and Walker [177], and was later studied in detail by Halstead et al. [61–63], Walker et al. [181] and many others. Wake-induced transition has often been assumed to be of the bypass type, where the initial stages of natural transition are bypassed, including the inception and growth of Tollmien–Schlichting (T–S) waves [111]. There is now evidence that instability waves can exist and grow in flows with significant free-stream disturbances. It should also be recognised that the term *bypass transition* now encompasses a wide range of breakdown mechanisms in flows where free-stream disturbances are present.

Instability wave packets were detected on the surface of a compressor stator by Hughes and Walker [85] using wavelet analysis of data from surface mounted hot-film sensors. The results from this analysis showed significant T–S wave packet activity prior to transition. The dominant wave frequencies were compared with linear stability predictions for the unstable T–S wave frequency having the greatest amplification rate (see Walker [176]). Reasonable agreement was found, considering that pressure gradient alters the frequency range of disturbances receiving amplification, and that maximum amplification ratio is a more appropriate parameter. This provided strong evidence for instability processes retaining a significant role in wake-induced transition

on compressor blades. Hughes and Walker [85] varied the free-stream turbulence level experienced by a blade element by clocking the upstream IGV blade wakes with respect to the stator blade row and observed wave packet activity in both low and high turbulence cases.

These observations are supported by Boiko et al. [13], who investigated the effect of free-stream turbulence on the transition of a flat plate boundary layer under zero pressure gradient was studied. They found that artificially introduced T–S waves not only received amplification, but were also involved in non-linear processes that contributed to the formation of turbulent spots.

Many recent studies of wall-bounded flows with high free-stream turbulence have shown that bypass transition involves elongated streaky structures that produce alternating regions of low and high velocity in the spanwise direction [6, 16]. These structures are thought to result from free-stream turbulence interacting with the boundary layer during a receptivity stage. Zaki et al. [197] observed similar flow structures on a compressor pressure surface in a DNS study of a linear compressor cascade. Once initiated the structures grow in size with the boundary layer. Their propagation velocity is typically $0.7U$, which is characteristically different from T–S wave velocity of between $0.4U$ and $0.5U$. Several different modes of instability have been associated with these streaky structures. Recent research suggests that the mode responsible for breakdown to turbulence depends largely on flow conditions [6, 16]. There is also a suggestion that streaky structures may interact with T–S waves resulting in new disturbances [8], or may be accompanied by three-dimensional T–S wave packets [12].

Unsteadiness in low turbulence free-stream flow can also lead to the formation of instability wave packets. Obremski and Fejer [121] studied boundary layer transition on a flat plate with a periodically oscillating free-stream velocity. Instability waves appeared in hot-wire data near the phase corresponding to minimum velocity; this would most likely correspond to the greatest destabilisation of the boundary layer. The convection speed and growth rate of the wave packets were very similar to classic two-dimensional T–S waves observed in other studies. Similar wave packets were artificially generated in a flat plate flow with zero pressure gradient by Cohen et al. [22].

Unsteady flow in turbomachinery can result from a number of possible sources (see Chapter 5). Michelassi et al. [116] used LES to study wake perturbed flow through a linear turbine cascade. Upstream wakes were observed to interact with the blade lead-

ing edge to produce elongated counter rotating vortices close to the pressure surface. These studies and others [93, 159] suggest that unsteady flow occurring at the leading edge of turbomachine blades plays a significant role in transition and boundary layer development.

This chapter studies unsteady transitional flow at the leading edge of both C4 and CD stator blades. The first part examines the influence of passing rotor wake disturbances on laminar boundary layer stability at the leading edge of both C4 and CD stator blades. Numerical simulations performed using an unsteady quasi three-dimensional flow solver, UNSFLO, are validated by comparing predicted skin friction with experimental measurements of quasi wall shear stress obtained from surface hot-film sensors. The simulations show that rotor wake chopping has a destabilising effect on the suction surface and a stabilising effect on the pressure surface.

Measurements from surface mounted hot-film sensors on the stator blades are examined for transitional flow phenomena occurring near the leading edge. Disturbances observed in the measurements are examined for their relative frequency and propagation velocity, and the manner in which they are influenced by axial blade row spacing, compressor loading, turbulence, and random variations in the amplitude of blade wake disturbances.

Parts of this chapter relating to transitional flow phenomena at a C4 stator blade leading edge were published in Henderson et al. [68]. An independent study of the flow around a CD stator of differing geometry was concurrently published by Wheeler et al. [187]. Detailed flow measurements in the latter study were made in a low-speed research compressor. Wakes from upstream rotor blades were observed to interact with the stator blade near the leading edge, forming a thickened region of laminar boundary layer that travelled along the suction surface at a mean velocity of $0.7U$. Turbulent spots were formed within this structure a short distance downstream, initiating a wake-induced transitional strip. In many respects, these observations support and reinforce the main findings of the present study.

8.1 Scope of Experimental Investigation

In this chapter, measurements from both C4 and CD stator blades are studied for flow phenomena occurring at the leading edge. A matrix of test cases was constructed to study a range of effects, including turbulence level, axial spacing and compressor

loading. All hot-film measurements on the C4 stator blade were made earlier by Hughes [83]; some of these are described and presented in Chapter 6. The hot-film measurements on the CD stator blade are presented in Chapter 7. The matrix of test cases is shown in Table 8.1.

Test Case	Stator Blade	Inlet Grid	Axial Gap	Clocking Case (a/S)	Test Flow Coefficients (ϕ)
A	C4	No	LAG	0.5	0.600, 0.675, 0.840
B	C4	No	LAG	0.0	0.600, 0.675, 0.840
C	C4	No	SAG	0.5	0.600, 0.675, 0.840
D	C4	No	SAG	0.0	0.600, 0.675, 0.840
E	CD	Yes	SAG	0.0	0.600, 0.675, 0.750

Table 8.1: Matrix of test conditions for the study of the flow around the leading edge of the C4 and CD stator blades. All measurements were made at constant reference Reynolds number ($Re_c = 120000$)

The turbulence level experienced by the C4 stator blade for the low inlet turbulence measurements of Hughes [83] was varied using two relative clocking positions between IGV and stator blade rows. Chapter 6 compared transitional flow behaviour on the stator surface at low inlet turbulence with measurements at high inlet turbulence generated by the turbulence grid. Clocking the IGV wakes in the stator passage ($a/S = 0.5$, Case A) resulted in strong periodic transitional flow on the stator blade surface. Aligning the IGV wakes on the stator blade row ($a/S = 0.0$, Case B) was found to give similar transitional flow behaviour to using the turbulence grid and aligning the IGV wakes in the stator blade passage. The CD stator was tested at high inlet turbulence with the grid and also with immersion in IGV wake turbulence ($a/S = 0.0$, Case E).

Hughes [83] also made hot-film measurements using the large and short axial gap configurations of the research compressor. These gave relative spacings based on C4 stator chord of 41% c and 106% c . The axial spacing used in the study of the CD stator was 18.4% c (based on CD stator chord length). Gorrell et al. [52] studied the performance of a transonic compressor for three different axial spacings: close (10% c), mid (26% c) and far (55% c). Gorrell et al. [52] reported the mid and far spacings were representative of current design practice. Lower spacing are desirable to reduce weight and may improve efficiency, however reducing spacing too much leads to increased noise and vibration.

The effect of loading was investigated in each of the five test cases. Three compressor loading cases were used for studies with the C4 stator, as previously discussed in Chapter 6: high ($\phi = 0.600$), medium ($\phi = 0.675$) and low ($\phi = 0.840$). The same loading cases were used with the CD stator, with the exception of the low loading case, where a flow coefficient of $\phi = 0.750$ was chosen.

All measurements presented in this chapter were made at a constant reference Reynolds number of $Re_c = 120000$.

8.2 Unsteady Flow Simulation

8.2.1 The UNSFLO Solver

The UNSFLO suite of programs developed by Giles and Haines [50] were designed to study unsteady flow interactions between adjacent blade rows in compressors and turbines. The flow solver uses a hybrid approach that solves the thin layer Navier–Stokes (N–S) equations on an O-mesh around each blade element, and the inviscid Euler equations over the remaining flow domain. The Euler equations are solved with second-order accuracy on an unstructured mesh using the Lax–Wendroff algorithm. The N–S equations are solved using an alternating direction implicit method with flux splitting. This gives third-order upwinding for the residual operator and first-order upwinding for the implicit operator. Further description of the code and validations may be found in references [49, 50, 58].

The numerical scheme used by the UNSFLO solver neglects viscous dissipation in wakes convecting through the free-stream flow. However, Giles and Haines [50] argue this is compensated to some extent by artificial dissipation in the numerical scheme. This uncertainty was not considered to be critical in this study since the simulated wake properties were carefully modelled at the compressor leading edge and the study was primarily concerned with the flow development close to the leading edge.

There was a two-fold advantage in using the UNSFLO solver for analysing the flow around stator blade leading edges. First, although a differential form of the N–S equations are solved on the O-mesh, the structured mesh allows calculation of integral boundary layer parameters, thus allowing boundary layer stability to be studied. Second, the solver features an algebraic turbulence model, which allows the location of laminar–turbulent boundary layer transition to be arbitrarily specified on each blade surface.

8.2.2 Model Description

The UNSFLO solver was used to model the unsteady flow through a single outlet stator blade row in the UTAS research compressor. The respective inlet and outlet locations for the C4 stator model were 25% c axially upstream from the blade leading edge and 25% c axially downstream from the trailing edge (based on C4 chord length). The same relative spacings were used for the CD stator model. The unstructured mesh of quadrilateral elements surrounding the O-mesh contained approximately 300 elements in the axial direction and 100 in the peripheral direction. The structured O-mesh contained approximately 450 elements around each stator blade and 30 elements in the normal direction. Closure of the Reynolds-averaged Navier–Stokes equations was achieved using the algebraic turbulence model of Cebeci and Smith [19]. The specified locations for transition inception were estimated from the steady flow quasi three-dimensional MISES flow solver of Drela and Giles [36].

Transition in the C4 stator model occurred well downstream from the leading edge and was not considered to significantly influence the unsteady laminar flow development in the region of interest around the leading edge. Transition in the CD stator model was fixed downstream from peak-suction on the suction surface and near the blend point on the pressure surface. The hot-film measurements presented in Chapter 7 showed that transition on the pressure surface did not vary significantly during the rotor passing period.

The incoming rotor wakes were modelled by prescribing a moving velocity defect at the model inlet plane. The wake model parameters were carefully selected to give wake width and velocity defect values in the plane of the stator leading edge compatible with values predicted using a steady flow model over the same distance, and hot-wire measurements of absolute velocity fluctuations; this avoided errors that could be introduced by an unknown level of numerical diffusion acting on the wakes as they convect through the model domain. This simple approach does not account for viscous wake stretching effects which may arise due to blade circulation effects in the blade-blade plane, radial variations of whirl velocity, and modification of mixing processes by interaction with wakes from upstream blade rows. However, the model should give a rough approximation of an ensemble-averaged perturbation seen by the stator leading edge corresponding to the low turbulence clocking case with the IGV wake streets aligned in the stator passage ($a/S = 0.5$).

The wake model was based on the experimental data and velocity defect profile given by Schlichting [147] as

$$\frac{\Delta u}{U}(x, y) \approx 0.98 \left(\frac{C_d d}{x} \right) \left[1 - \left(\frac{y}{b} \right)^{3/2} \right]^2 \quad (8.1)$$

where $\Delta u = U - u$ is the wake velocity defect at a distance y normal to the wake centreline and x downstream from the wake source. The half-width of the wake is given by $b \approx 0.567\sqrt{C_d x d}$. The wake angle in the rotor relative frame was determined from time-averaged flow angle measurements using a three-hole probe. The wake profile given by Eq. (8.1) was found to agree well with numerically simulated wakes in a recent study by Wu et al. [194]. The resulting absolute velocity fluctuations are consistent with experimental observations of rotor wake disturbances in the UTAS research compressor reported by Boxhall [15].

The long axial spacing configuration in the research compressor has the advantage of allowing detailed measurement of unsteady flow phenomena such as IGV-rotor wake-wake interactions. It also effectively decouples the rotor and stator pressure fields. As a result, the unsteady flow experienced by stator blades is essentially dominated by convective disturbances from the upstream rotor wakes rather than pressure field effects. This simplifies the analysis and validation of the numerical model. The numerical predictions are subsequently applied to investigate the unsteady flow behaviour at more practical values of axial blade row spacing, such as the short axial gap configuration of the research compressor.

Due to the large number of variables under investigation, results from the numerical analysis will only be presented for the medium loading case ($\phi = 0.675$). This condition corresponds to near design point operation for both the C4 and CD stators.

8.2.3 Model Results

Figures 8.1–8.3 show instantaneous UNSFLO solutions around the C4 and CD stator leading edge at medium compressor load ($\phi = 0.675$) for four phases during the rotor wake passage.

These figures may be interpreted to provide useful information about the unsteady flow behaviour. In each figure, the stator blade is oriented so that the suction surface is the lower surface and the direction of the free-stream flow is from top-left to bottom-right. The vectors show the instantaneous deviation of unsteady flow velocity from

the time-mean flow.

The following general observations may be made. The incoming rotor wakes are clearly indicated by both elevated levels of entropy and the unsteady velocity vectors. An observer moving with the free-stream sees a reverse flow within a wake region that is commonly referred to as a ‘negative jet’ or ‘wake jet’ (see, for example [69, 163]). The negative jet associated with the rotor wake causes a relative convection of fluid towards the stator pressure surface and away from the stator suction surface.

At $t^* = 0.50$, the rotor wake centre is about $10\%c$ upstream of the stator leading edge and starts to exhibit distortion from the upstream potential flow field of the blade. At $t^* = 0.60$, the local flow deceleration along the stagnation streamline is clearly evident. The leading edge is completely immersed in the wake and the stator experiences a local increase in incidence that is largely confined to the first $5\%c$. Fluid entrainment by the negative jet decreases the suction surface velocity immediately prior to the wake arrival. Conversely, the discharge of the rotor wake jet onto the pressure surface causes an increase in velocity prior to the wake arrival. At $t^* = 0.70$, the rotor wake is about $10\%c$ downstream from the stator leading edge and $5\%c$ downstream from the CD stator leading edge. The perturbations at the leading edge are now minimal. The rotor wake has convected further on the suction surface due to the effects of the stator blade circulation. The negative jet causes a reduction in velocity after the wake passage on the pressure surface and an increase in velocity on the suction surface, as shown at $t^* = 0.80$. The streamwise extent of contact between the rotor wake fluid and the stator blade is clearly increasing on the pressure surface and decreasing on the suction surface. These phenomena were reported in numerical studies of flow through a compressor stage by Ho and Lakshminarayana [69]. Similar behaviour has been observed in turbine cascades except that the direction of the wake jet is reversed (e.g. [163]). These results show that the wake jet effect causes unsteady flow perturbations on both blade surfaces and entrainment of fluid by the jet causes large scale vortical flows throughout the blade passage.

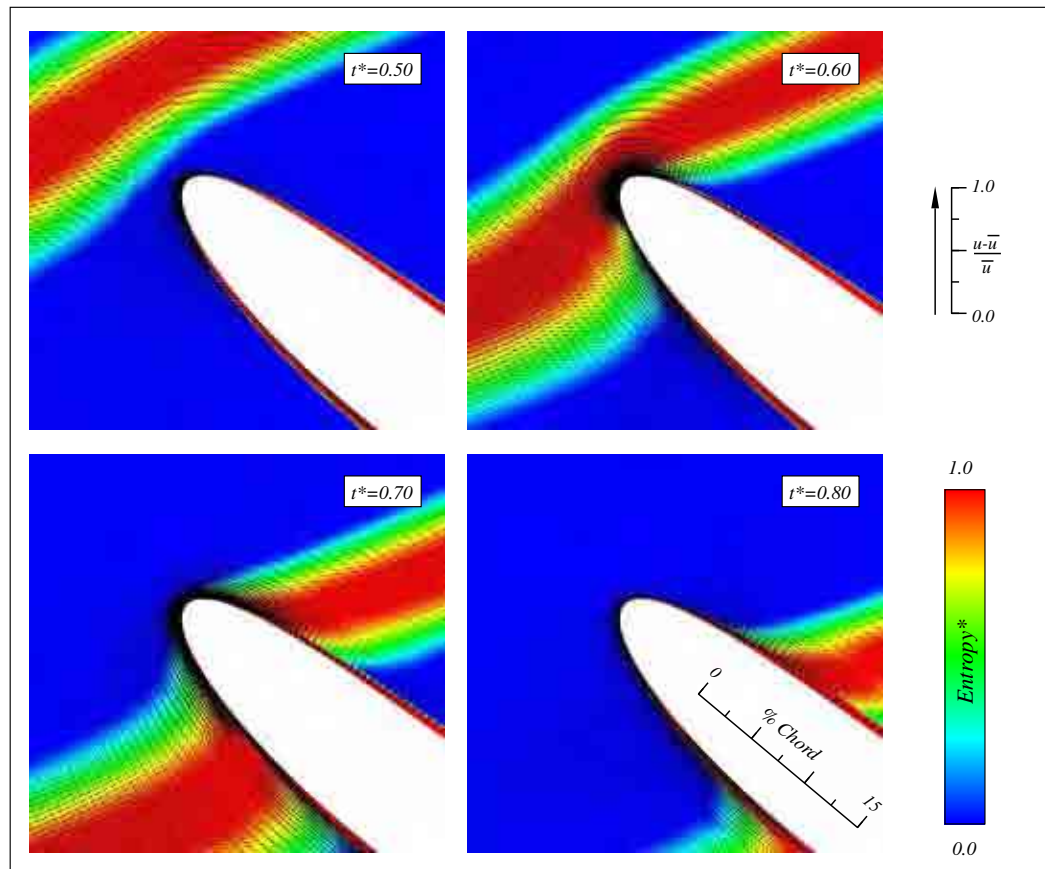


Figure 8.1: Unsteady flow field around C4 stator leading edge (UNSFLO) for LAG configuration (Case A, $\phi = 0.675$, $Re_c = 120000$). Vectors indicate perturbation from local time-mean velocity. Colour shading indicates fluid entropy relative to the maximum level at the wake centre

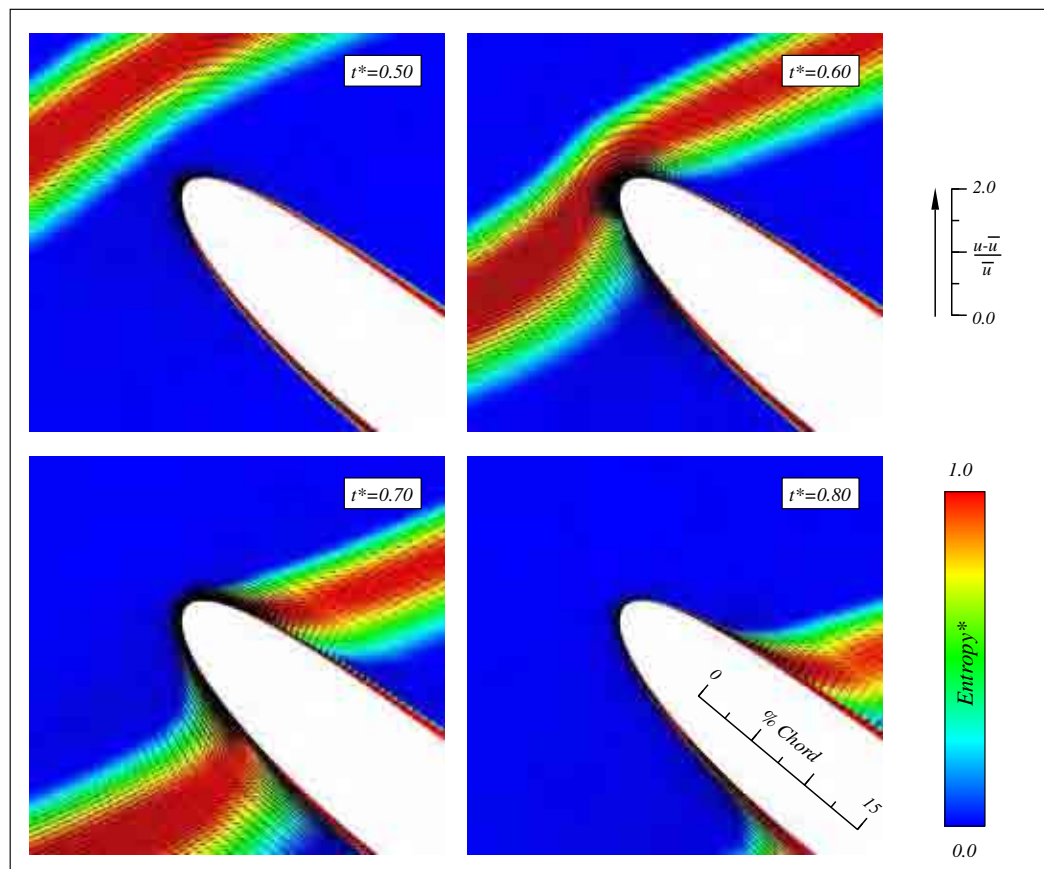


Figure 8.2: Unsteady flow field around C4 stator leading edge (UNSFLO) for SAG configuration (Case C, $\phi = 0.675$, $Re_c = 120000$). Vectors indicate perturbation from local time-mean velocity. Colour shading indicates fluid entropy relative to the maximum level at the wake centre

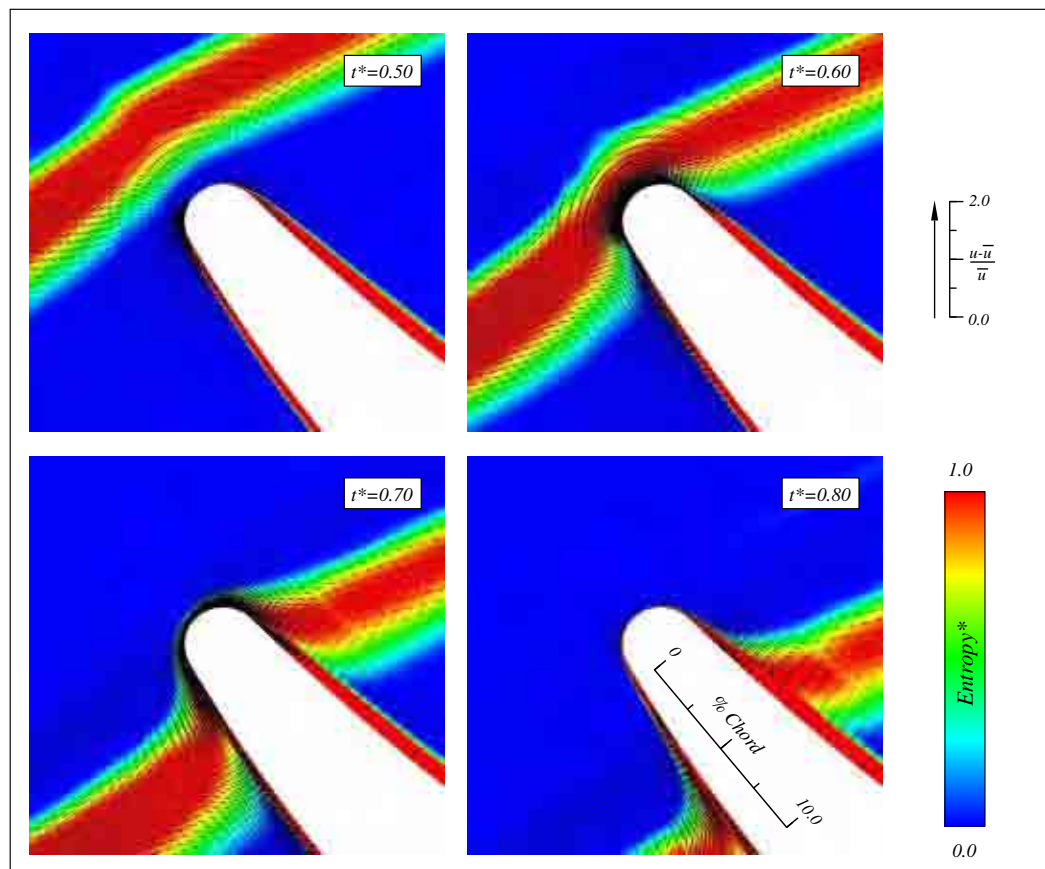


Figure 8.3: Unsteady flow field around CD stator leading edge (UNSFLO) for SAG configuration (Case E, $\phi = 0.675$, $Re_c = 120000$). Vectors indicate perturbation from local time-mean velocity. Colour shading indicates fluid entropy relative to the maximum level at the wake centre

8.2.4 Predicted Leading Edge Boundary Layer Behaviour

The UNSFLO solutions were analysed to provide information about the temporal variation in boundary layer properties near the stator leading edge. The right-hand side of Figs 8.4–8.6 show the temporal variation in dimensionless skin friction factor (c_f/\bar{c}_f) at several stations around the leading edge. Here \bar{c}_f represents a time-average over the rotor blade passing period. The fluctuations correlate well with the centre of the rotor wake $s^* \sim t^*$ trajectory as indicated by the dashed line. The fluctuations are also consistent with the qualitative descriptions made in Section 8.2.3. The left-hand side of each figure shows experimental hot-film measurements made at similar surface positions to the UNSFLO results. The hot-film measurements have been expressed in terms of dimensionless ensemble-averaged quasi wall shear stress ($\langle\tau_q\rangle/\bar{\tau}_q$); this non-dimensionalisation reduces uncertainty from the approximations inherent in Eq. (4.11).

The shear stress perturbations observed in both the experimental and UNSFLO results agree well in terms of shape and character for the region of laminar flow close to the leading edge. On the C4 stator, the agreement starts to deteriorate at $s^* = 0.118$ on the suction surface, where the effects of diffusion from wake-induced turbulence are starting to become evident in the experimental data. On the CD stator, the boundary layer is separated at $s^* = -0.033$ on the pressure surface, causing large fluctuations in $\langle\tau_q\rangle/\bar{\tau}_q$. The UNSFLO solver also predicts separation at this location; here, the fixed transition location in the numerical model appears to dampen oscillations in the boundary layer that are evident in the hot-film data. Excluding records very close to the time-mean stagnation point location, it is seen that the wake-induced shear stress fluctuations are of opposite phase on the suction and pressure surfaces: there is a decrease in wall shear stress along the wake path on the suction surface and a corresponding increase on the pressure surface near the leading edge.

Figures 8.7–8.8 show computed values of momentum thickness Reynolds number Re_θ and shape factor H at several positions around the leading edge of each stator blade. The thin boundary layer responds almost instantly to the unsteady flow perturbation, as noted in other studies [129, 187]. On the suction surface, the flow perturbation caused by the passing wakes causes simultaneous increases in both Re_θ and H . This indicates that the boundary layer will be periodically destabilised by the passing wakes as increases in Re_θ and H are both individually destabilising.

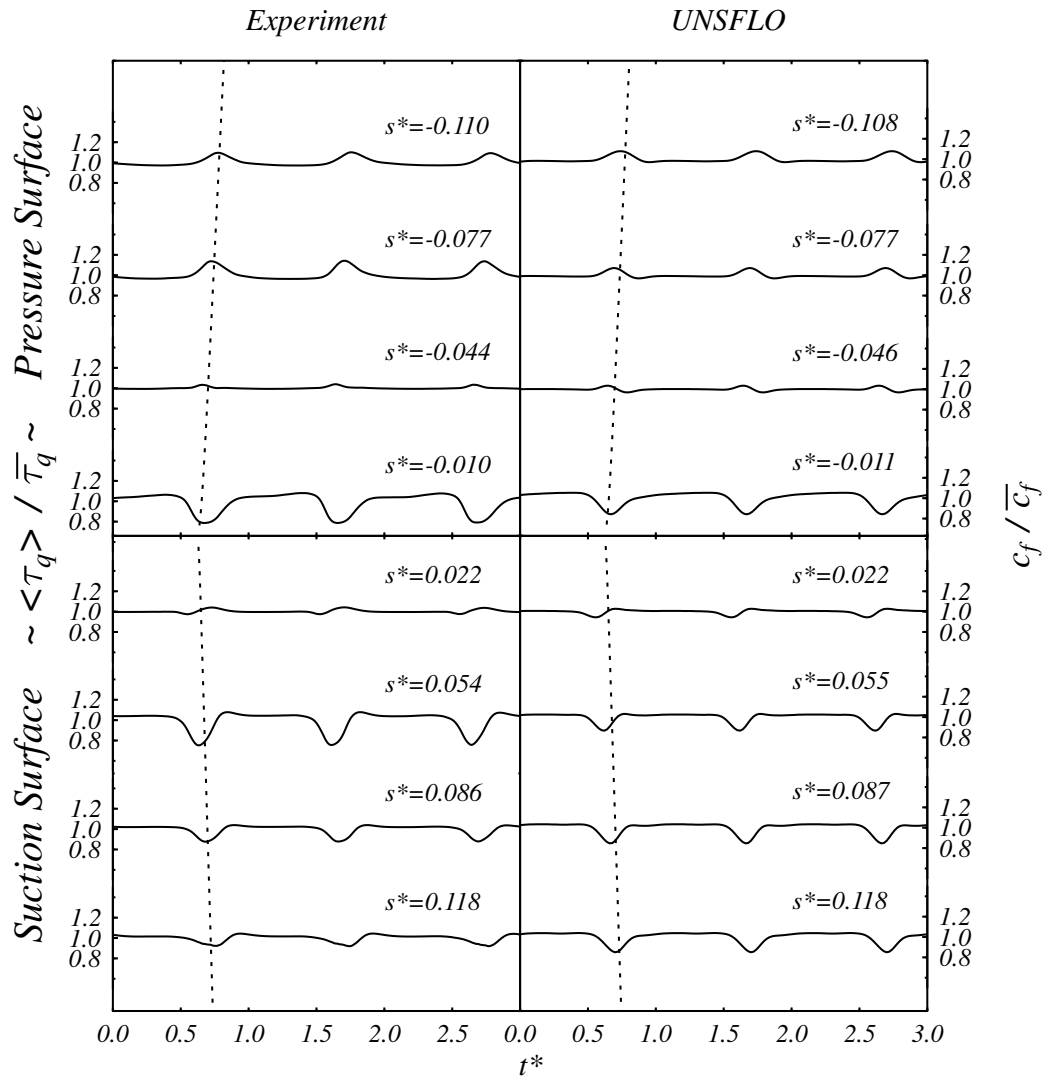


Figure 8.4: Comparison of dimensionless ensemble-averaged quasi wall shear stress $\langle \tau_q \rangle / \bar{\tau}_q$ from hot-film sensors (left) and dimensionless skin friction factor c_f / \bar{c}_f from UNSFLO (right). C4 stator, LAG configuration, Case A, $\phi = 0.675$, $Re_c = 120000$

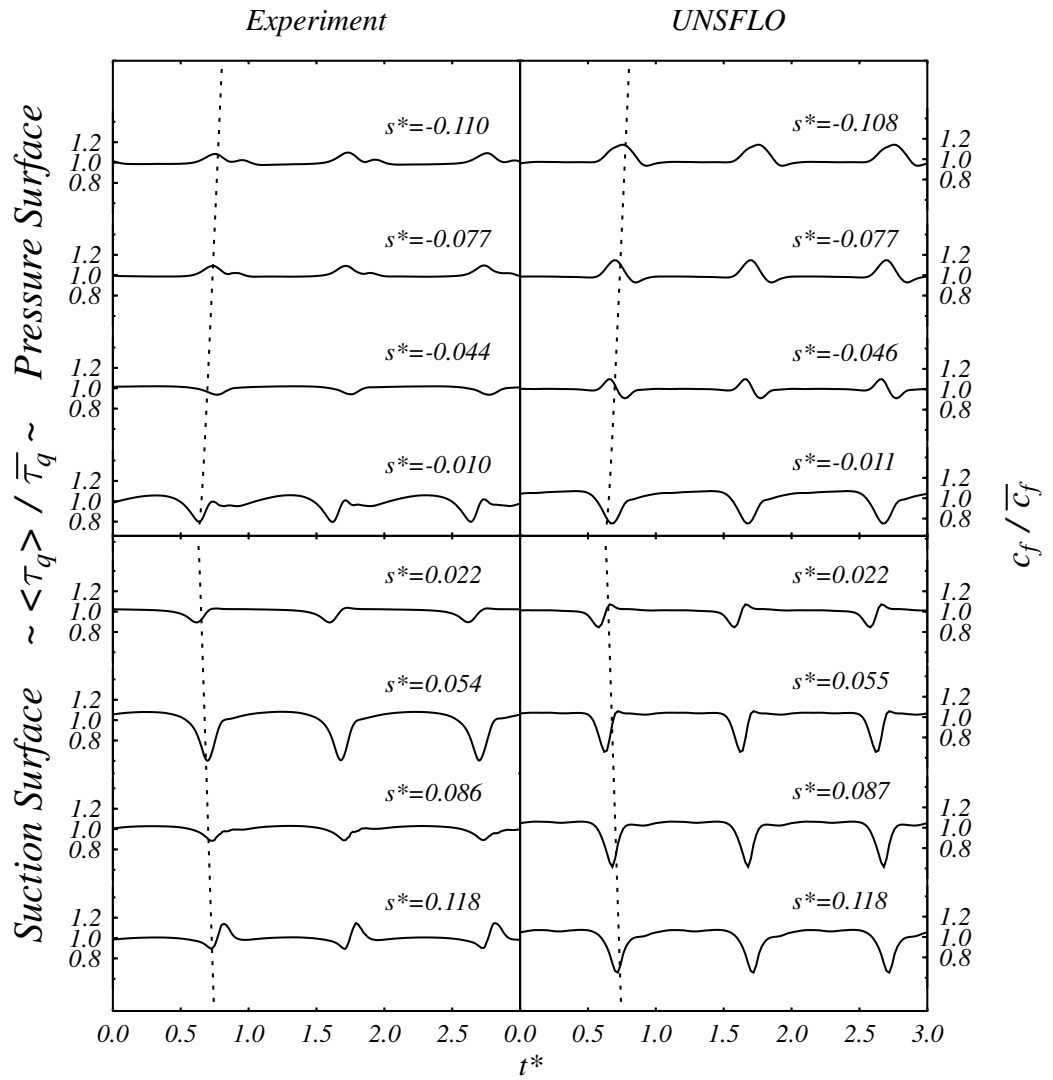


Figure 8.5: Comparison of dimensionless ensemble-averaged quasi wall shear stress $\langle \tau_q \rangle / \bar{\tau}_q$ from hot-film sensors (left) and dimensionless skin friction factor c_f / \bar{c}_f from UNSFLO (right). C4 stator, SAG configuration, Case C, $\phi = 0.675$, $Re_c = 120000$

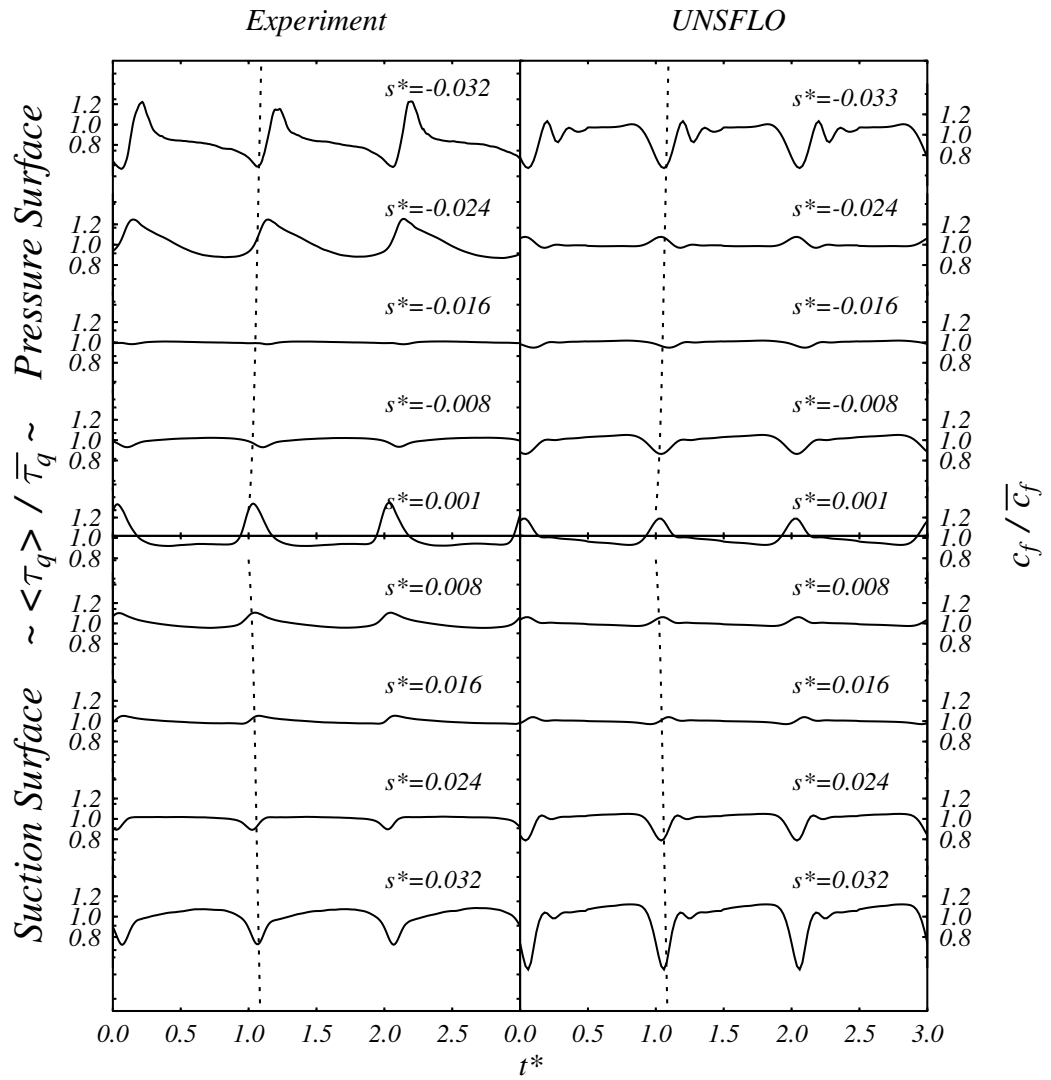


Figure 8.6: Comparison of dimensionless ensemble-averaged quasi wall shear stress $\langle \tau_q \rangle / \bar{\tau}_q$ from hot-film sensors (left) and dimensionless skin friction factor c_f / \bar{c}_f from UNSFLO (right). CD stator, SAG configuration, Case E, $\phi = 0.675$, $Re_c = 120000$

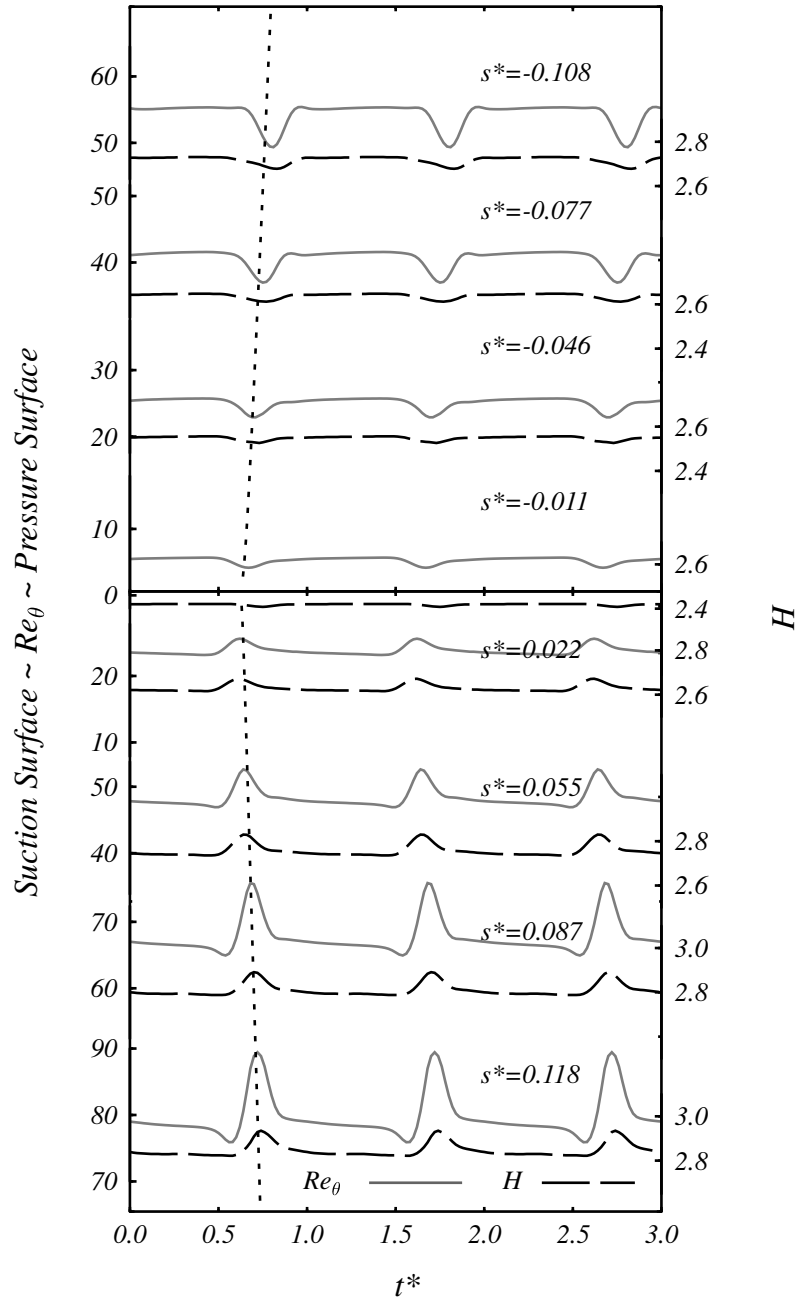


Figure 8.7: Temporal variation in momentum thickness Reynolds number and shape factor from UNSFLO computations. C4 stator, LAG configuration (Case A, $\phi = 0.675$, $Re_c = 120000$)

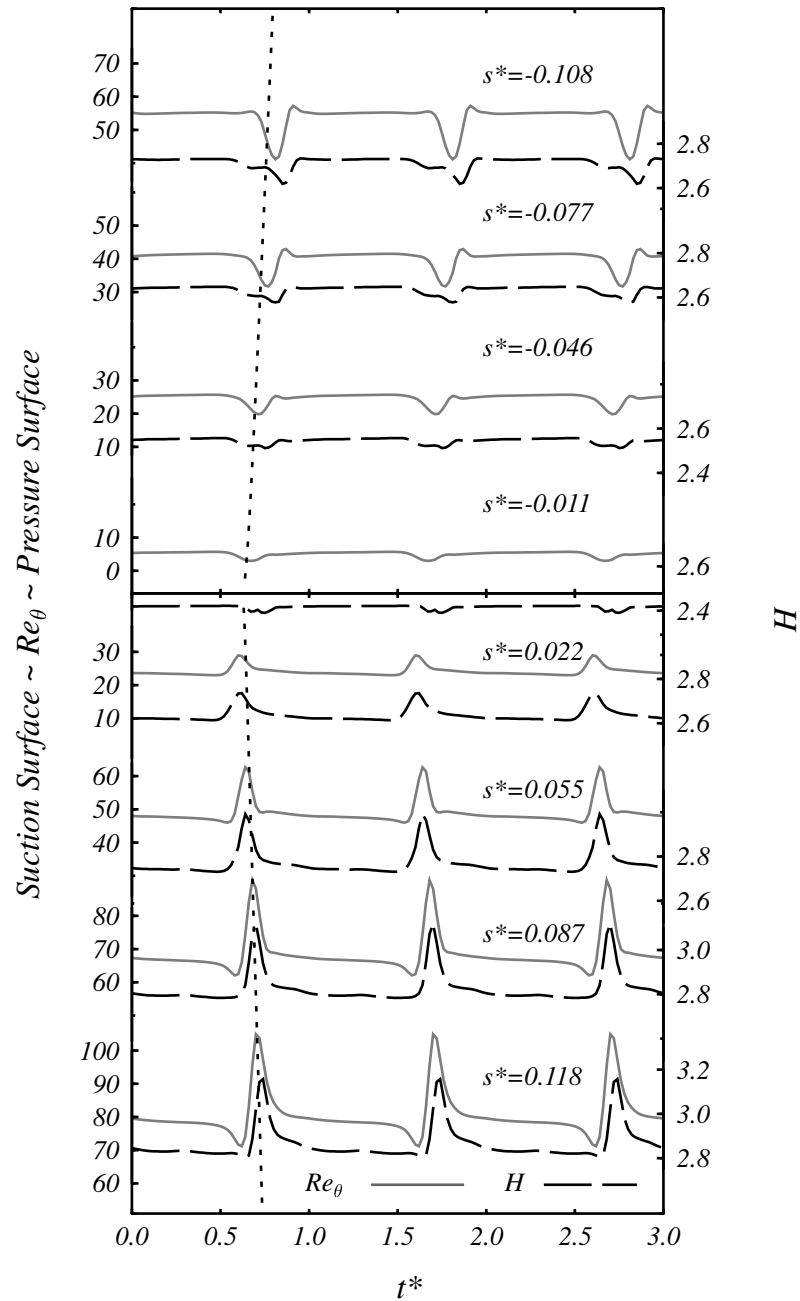


Figure 8.8: Temporal variation in momentum thickness Reynolds number and shape factor from UNSFLO computations. C4 stator, SAG configuration (Case C, $\phi = 0.675$, $Re_c = 120000$)

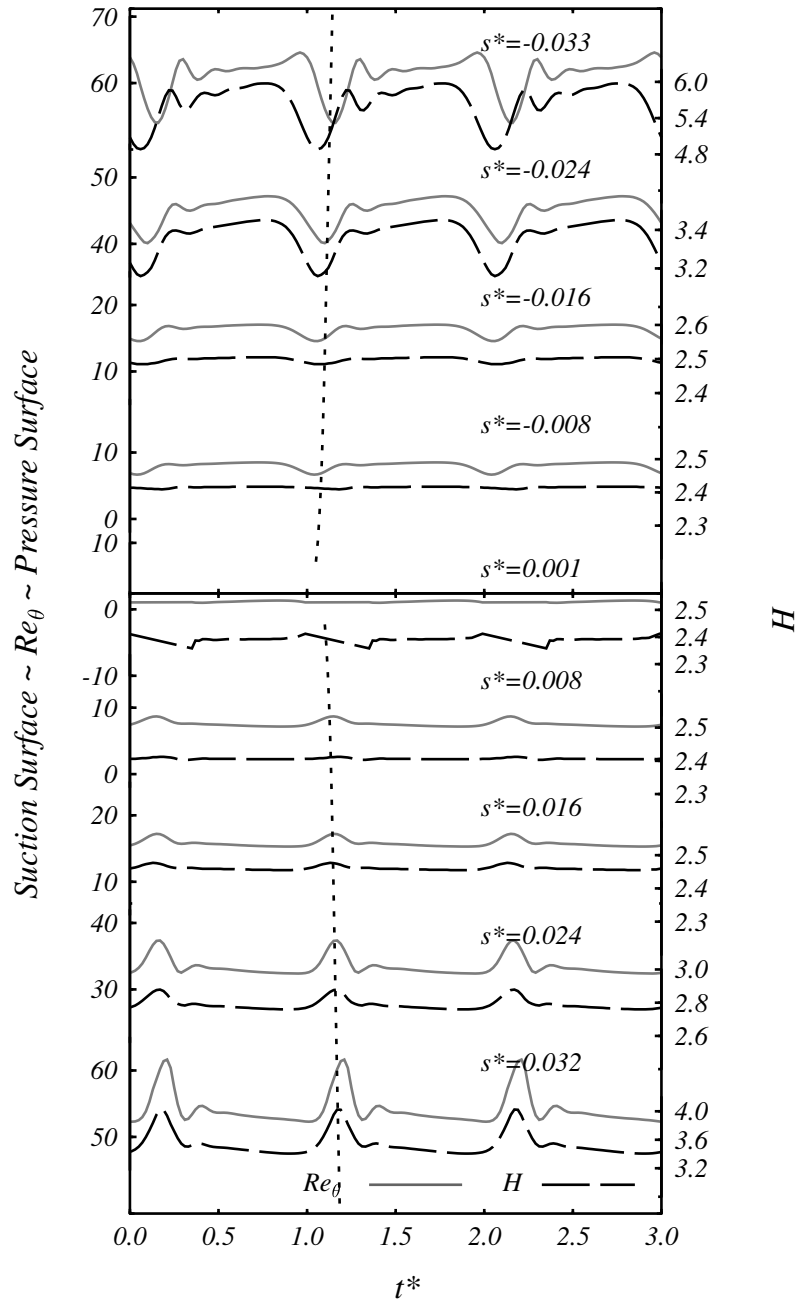


Figure 8.9: Temporal variation in momentum thickness Reynolds number and shape factor from UNSFLO computations. CD stator, SAG configuration (Case E, $\phi = 0.675$, $Re_c = 120000$)

While this effect may not be sufficiently strong to cause local transition, the unsteady flow perturbation will provide suitable conditions for the earlier appearance and enhanced growth of T-S type wave packets similar to those observed in the unsteady flow flat plate experiments of Obremski and Fejer [121] and the compressor blade studies of Hughes and Walker [85].

The resultant temporal variation of the neutral stability boundary on the stator suction surface was predicted from the computed unsteady momentum thickness Reynolds number and shape factor on a quasi-steady assumption using the approximate correlation for critical boundary layer Reynolds number $Re_{\theta_{cr}}$ given in Eq. (8.2). The results are shown on dimensionless time \sim space ($t^* \sim s^*$) plots in Figs 8.10–8.14. The approximate correlation for $Re_{\theta_{cr}}$ was obtained by regression analysis of data given in references [120, 140]. This may be written as

$$\log_{10}(Re_{\theta_{cr}}) = 4.018 - 2.77 \exp(-7100H^{-10}), \quad 2.2 \leq H \leq 4.0 \quad (8.2)$$

The results for the C4 stator are shown Figs 8.10–8.13 along with observations of wave packet occurrence and intermittency from Hughes and Walker [85]. The predicted neutral stability boundary precedes the wave packet occurrence on both the surfaces. On the pressure surface, the boundary layer shape factor and momentum thickness Reynolds number are both predicted to decrease during the rotor wake passage. This effect will be stabilising, however the magnitude of the boundary layer fluctuations on the pressure surface are much less than on the suction surface, and the resulting fluctuations in the neutral stability boundary are less significant.

The predicted fluctuations in the neutral stability boundary are greater for the short axial gap (SAG) cases, due to the stronger wake perturbation experienced at the stator leading edge. The greatest fluctuations of the predicted neutral stability boundary occur at low loading on the suction surface. Here the extensive region of accelerating flow near the leading edge gives rise to large variations in $Re_{\theta_{cr}}$ in response to the wake perturbations.

The results of wavelet analysis performed on hot-film data from the CD stator are shown in Fig. 8.14. At medium and low loading, wave-packet activity is detected on the suction surface prior to onset of the wake-induced transitional strip, as observed on the C4 stator. At high loading the wake-induced transitional strip occurs very close to the leading edge and no significant instability wave activity is detected.

The predicted neutral stability point on the CD stator occurs at the leading edge in both the high and medium loading cases. At low loading, the suction surface velocity spike is not sufficiently large to meet the neutral stability criterion; it is instead reached further along the suction surface. The use of a fixed transition location is thought to have a damping effect on the flow development in this region, limiting the movement of neutral stability point. There is a marked difference from the C4 low loading case in that instability wave activity now clearly precedes the predicted neutral stability boundary on the suction surface. This wave activity originates from the location of rotor wake impact on the leading edge; it propagates at a mean velocity of $0.7U$, which is suggestive of bypass transition becoming dominant.

8.2.5 Effect of Varying Rotor–Stator Axial Spacing

The effect of varying axial spacing may be seen by comparing Figs 8.4 and 8.5. The SAG case is more typical of blade row spacing in a practical machine. This decrease in axial gap increases the relative velocity defect of the rotor wake at the stator leading edge from $\Delta u/U = 0.13$ to $\Delta u/U = 0.21$. The amplitude of shear stress fluctuations in response to rotor wake passing is greater for the SAG case, although the overall change is comparatively small. The hot-film observations at low turbulence ($a/S = 0.50$) in Fig. 8.15 show the variability of individual wake signatures resulting from random turbulent fluctuations within the wakes to be relatively much greater. At high turbulence ($a/S = 0.0$), the fluctuations in shear stress produced by free-stream turbulence are seen to approach the magnitude of those resulting from rotor wake disturbances. The fact that the free-stream turbulence is less effective in promoting transition than the wake disturbances is suggestive of a receptivity issue related to turbulence scale.

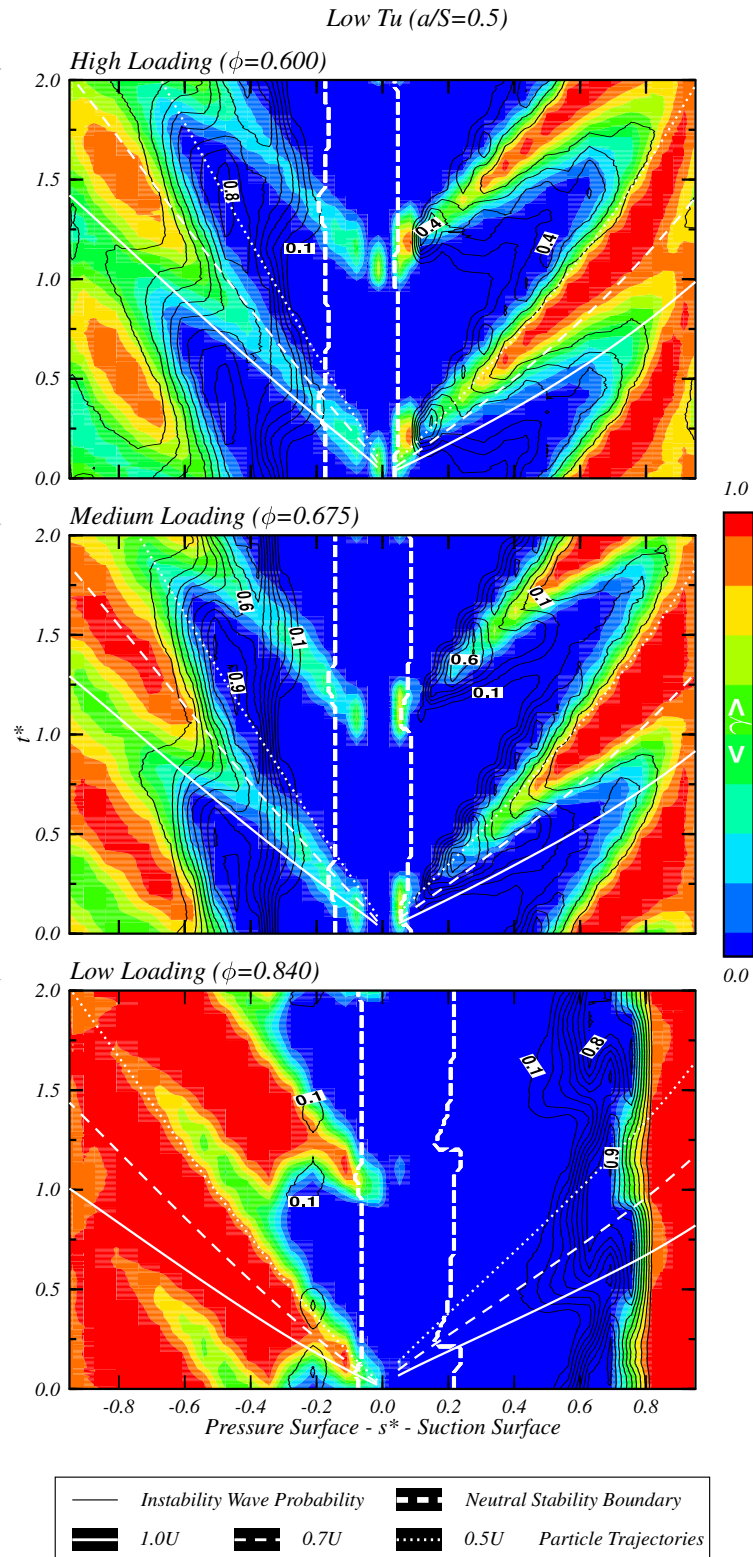


Figure 8.10: C4 stator surface ensemble-averaged intermittency (colour contours) and probability of instability wave occurrence (line contours) with superimposed particle trajectories at different proportions of local free-stream velocity (adapted from Hughes and Walker [85]) and added neutral stability boundary predicted by the present study (Case A, LAG, $Re_c = 120000$)

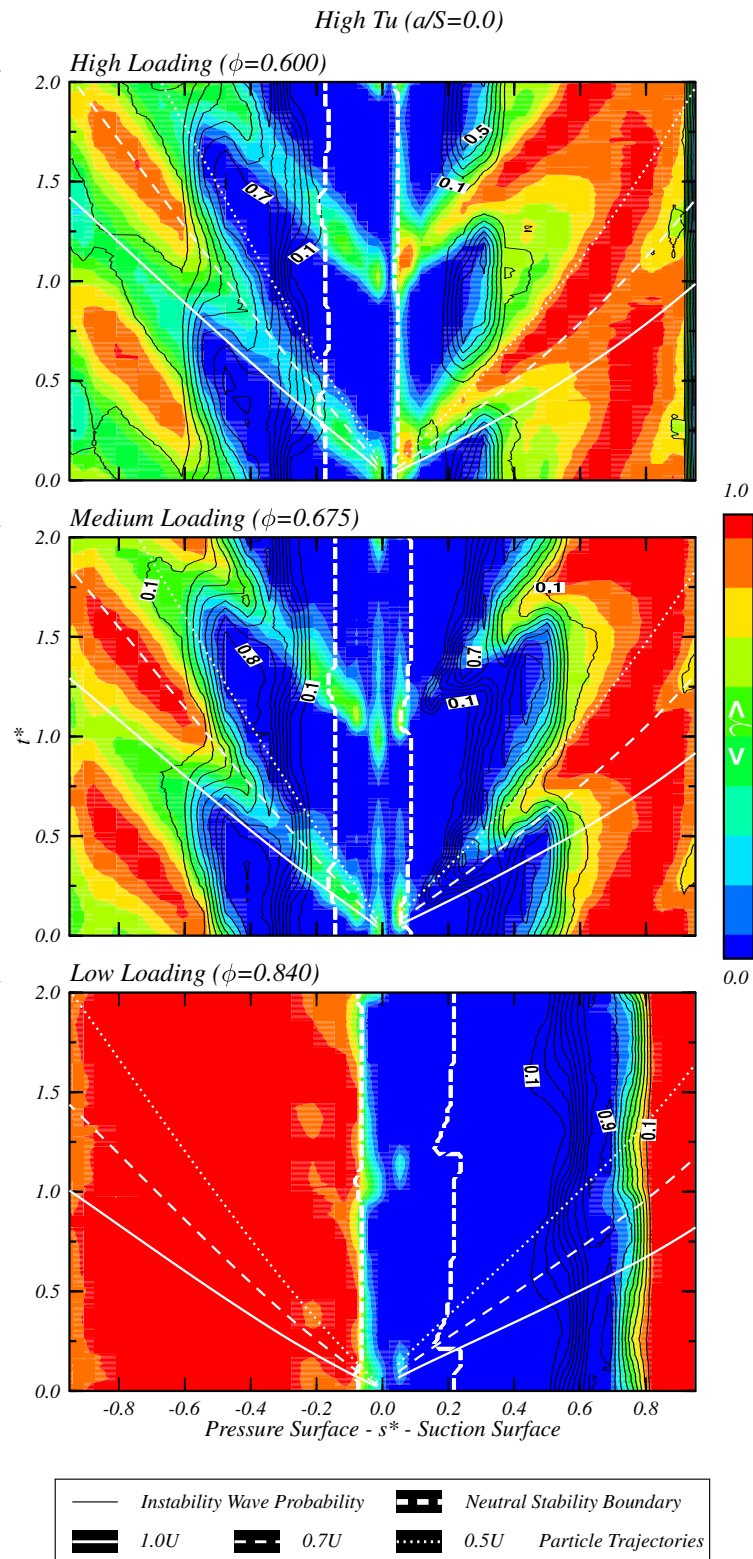


Figure 8.11: C4 stator surface ensemble-averaged intermittency (colour contours) and probability of instability wave occurrence (line contours) with superimposed particle trajectories at different proportions of local free-stream velocity (adapted from Hughes and Walker [85]) and added neutral stability boundary predicted by the present study (Case B, LAG, $Re_c = 120000$)

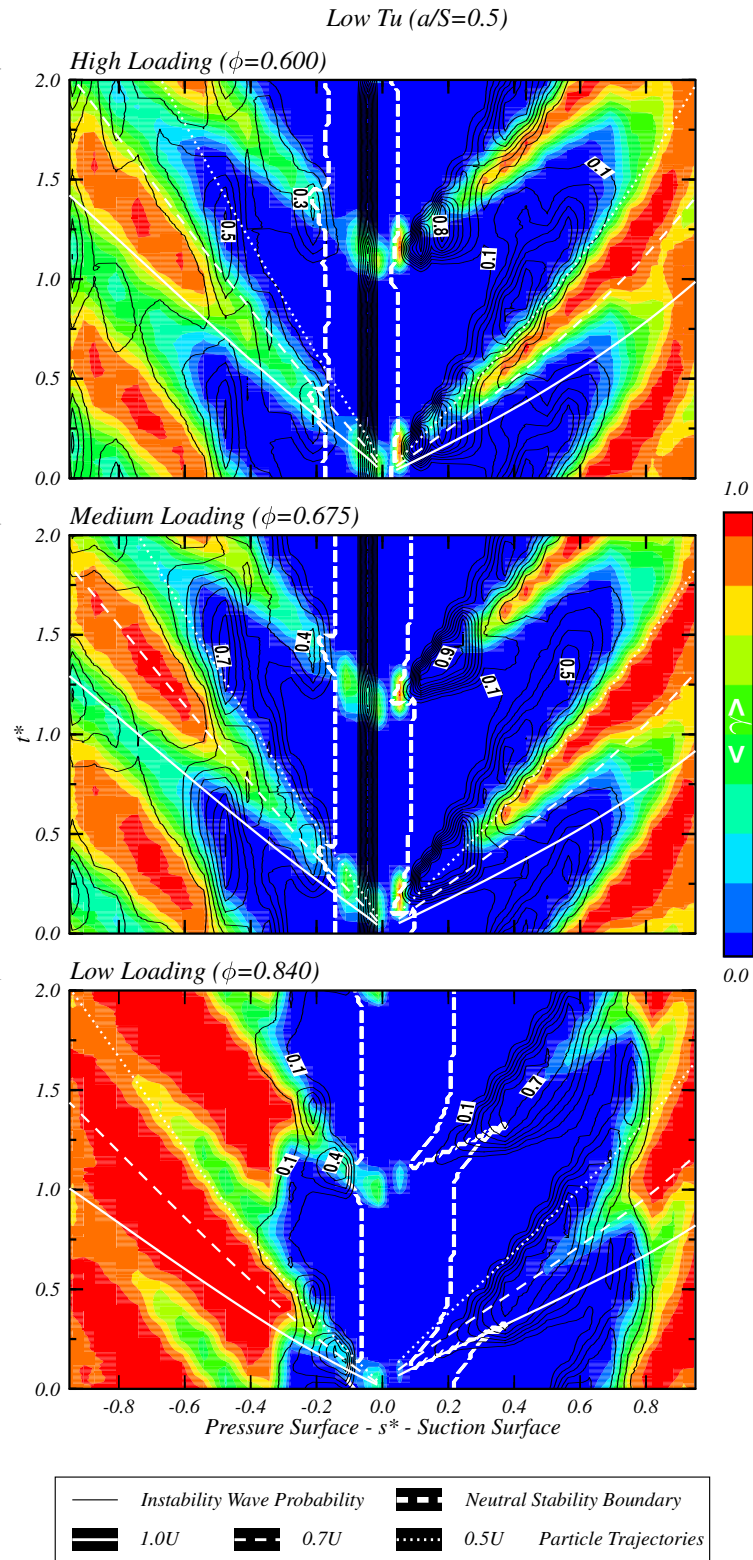


Figure 8.12: C4 stator surface ensemble-averaged intermittency (colour contours) and probability of instability wave occurrence (line contours) with superimposed particle trajectories at different proportions of local free-stream velocity and added neutral stability boundary predicted by the present study (Case C, SAG, $Re_c = 120000$)

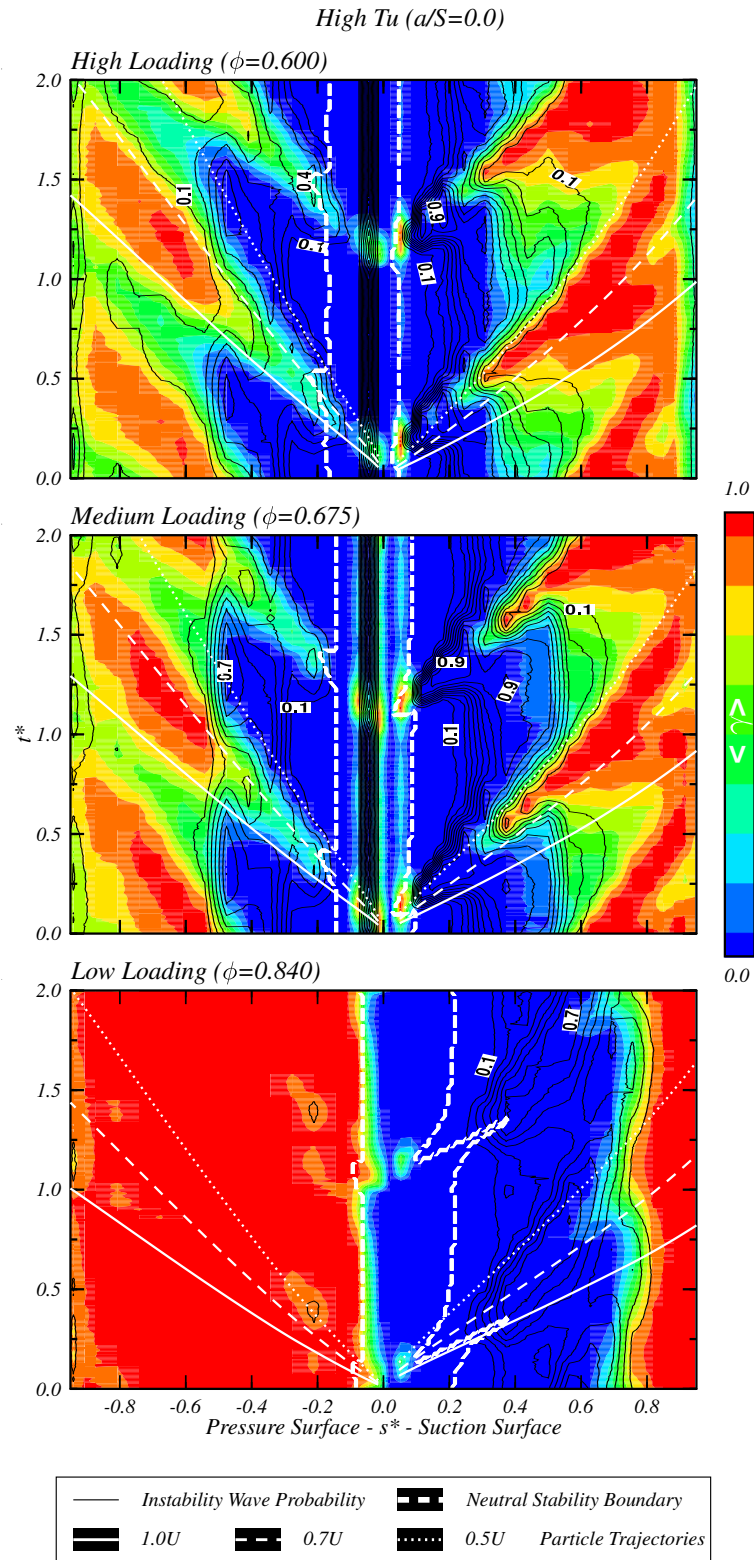


Figure 8.13: C4 stator surface ensemble-averaged intermittency (colour contours) and probability of instability wave occurrence (line contours) with superimposed particle trajectories at different proportions of local free-stream velocity and added neutral stability boundary predicted by the present study (Case D, SAG, $Re_c = 120000$)

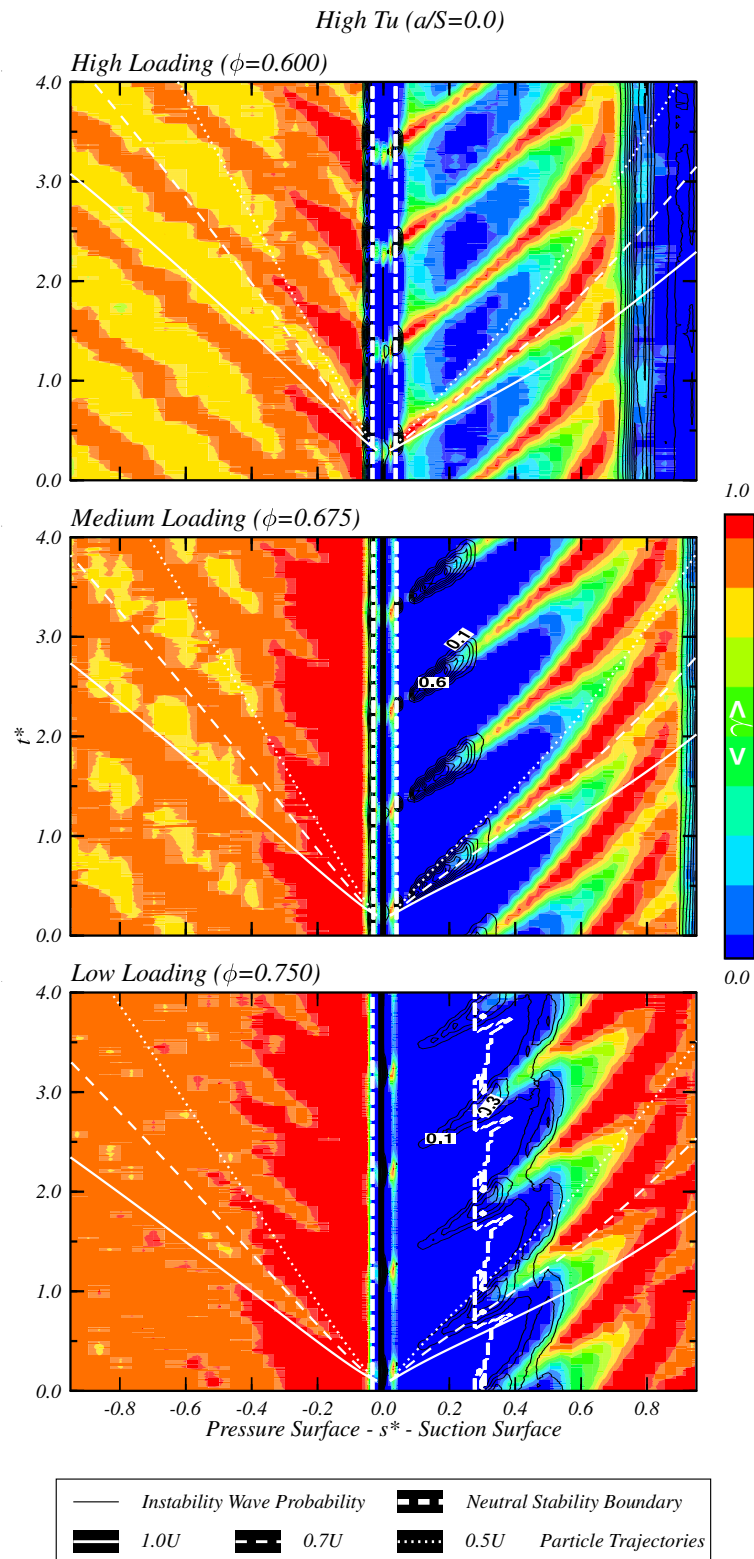


Figure 8.14: CD stator surface ensemble-averaged intermittency (colour contours) and probability of instability wave occurrence (line contours) with superimposed particle trajectories at different proportions of local free-stream velocity and neutral stability boundary predicted by the present study (Case E, SAG, $Re_c = 120000$)

8.3 Transitional Flow Observations

Further information about the flow development around the leading edge is provided by inspection of individual hot-film records. A collection of typical hot-film records for each of the five test cases is shown in Figs 8.15–8.17.

Each hot-film record was individually scaled to allow disturbance signatures to be followed along the blade surface. The numbering enclosed in brackets on the right-hand side indicates the dataset number at each hot-film sensor location. Records with equal numbering were acquired simultaneously. This is particularly useful in following the evolution of individual disturbances along the surface. Particle trajectories at speeds of $1.0U$, $0.7U$ and $0.5U$ have been overlaid for reference. In all cases, the data show considerable variability in both the amplitude and nature of wake-induced flow events.

8.3.1 C4 Stator

The long axial gap configuration with the C4 stator in Fig. 8.15 clearly shows the presence of instability wave packets on the suction surface in the medium and high loading cases (labelled event ‘A1’). These types of wave packets are similar to those observed by Hughes and Walker [85] and in studies by Obremski and Fejer [121] and Cohen et al. [22]. The convection speed of around $0.4 - 0.5U$ provides further confirmation that these are essentially T–S instability wave phenomena.

The T–S wave packets appear near the leading edge at instants coinciding with a local decrease in shear stress imposed by the wake jet interaction. Recent numerical studies by Zaki and Durbin [196] and co-workers have shown that inviscid Kelvin–Helmholtz instabilities are responsible for the final turbulent breakdown stage of bypass transition. However, these instability waves occur near the outer edge of the boundary layer and have a characteristically higher convection velocity: Zaki and Durbin [196] suggest a speed of about $\frac{2}{3}U$ for this secondary instability.

It is not clear if wave packets exist at the film sensor location of $s^* = 0.022$, since their frequency would likely exceed the cut-off frequency of the low-pass filtering. However, the strong acceleration around the leading edge ($s^* < 0.05$) would be expected to stabilise the boundary layer in this region. Transition resulting from this type of event only occurs after a relatively long period of wave amplification. The particular wave packet indicated by ‘A1’ in Fig. 8.15 eventually breaks down into a

turbulent spot at $s^* = 0.44$. Similar behaviour in the case of a more turbulent free-stream, when the stator blade is immersed in the IGV wake street ($a/S = 0.0$), is exhibited by event ‘A2’ in Fig. 8.15.

In the high load case, the traces show much greater periodicity in wake-induced transition. Breakdown occurs much more rapidly owing to the stronger adverse pressure gradient experienced by the flow.

Significantly different behaviour is exhibited by events ‘B1’ and ‘B2’ shown in Fig. 8.15 for the medium and low load cases respectively. Here the significant increase in shear stress characteristic of a turbulent spot appears quite quickly, with relatively little prior wave packet signature. The convection speed of these events is close to $0.7U$. Whilst characteristic of a turbulent spot, this propagation velocity is also consistent with the ‘turbulent puff’ events and the inviscid secondary instabilities in bypass transition reported by Zaki and Durbin [196]. These are packets of streamwise vortices (Klebanoff modes) induced principally by transverse and normal free-stream velocity fluctuations.

Boundary layer disturbances of this type were reported by Westin et al. [185] in response to isolated vortical disturbances introduced just upstream of a leading edge. A comprehensive description of instability phenomena and receptivity issues can be found in Boiko et al. [12]. It is possible for various types of instability to occur simultaneously and undergo complex interactions.

Wake-induced transition on the suction surface occurs more rapidly for the SAG configuration shown in Fig 8.16. Wave packet activity is not evident from visual inspection, as was noted in the LAG configuration, although wave packet activity was still detected using the wavelet analysis technique. As shown in Section 8.2.4, the stator experiences a stronger wake jet effect in the short axial gap configuration. This results in greater destabilisation of the boundary layer, as shown by the larger fluctuations of the neutral stability boundary. Increased destabilisation may contribute to a more rapid breakdown, being completed before T–S wave packet disturbances have grown to a visible magnitude on the blade surface.

Event ‘C’ observed on the stator suction surface at low load appears similar to event ‘B1’, in that it also convects with a speed of about $0.7U$. However, rapid transition does not occur, and the disturbance appears to be damped by the accelerating flow situation.

8.3.2 CD Stator

A collection of typical quasi wall shear stress records for the CD stator are shown in Fig 8.17. Additional measurements on the suction surface are shown in Figures 7.14–7.16.

In the high and medium loading cases, turbulent spots appear very close to the leading edge on the suction surface at about $s^* \approx 0.05$. There is little visible evidence of wave packet activity as was observed on the C4 stator in the LAG configuration. Flow structures are also observed near the leading edge in the low loading case, some of which develop into wake-induced spots further along the surface. In each loading case, the turbulent spots and flow structures are seen to originate at the rotor passing phase corresponding to minimum shear stress, where maximum destabilisation of the boundary layer is likely to occur. The convection velocity of these disturbances is generally around $0.7U$. Further discussion of flow phenomena on the CD stator suction surface is given in Section 7.6.4.

The flow on the pressure surface is mostly turbulent. The quasi wall shear stress record at $s^* = -0.032$ shows a near constant low level of shear stress with intermittent peaks. This is indicative of intermittent separation bubble behaviour. Flow structures are observed further along the pressure surface that move at speeds of typically $0.8U - 1.0U$. These are consistent with the flow perturbations observed on the pressure surface of the C4 stator; they reflect the impingement of the rotor wake jet, which causes a discharge of turbulent fluid onto the surface and an increase in local free-stream velocity immediately prior to the wake arrival.

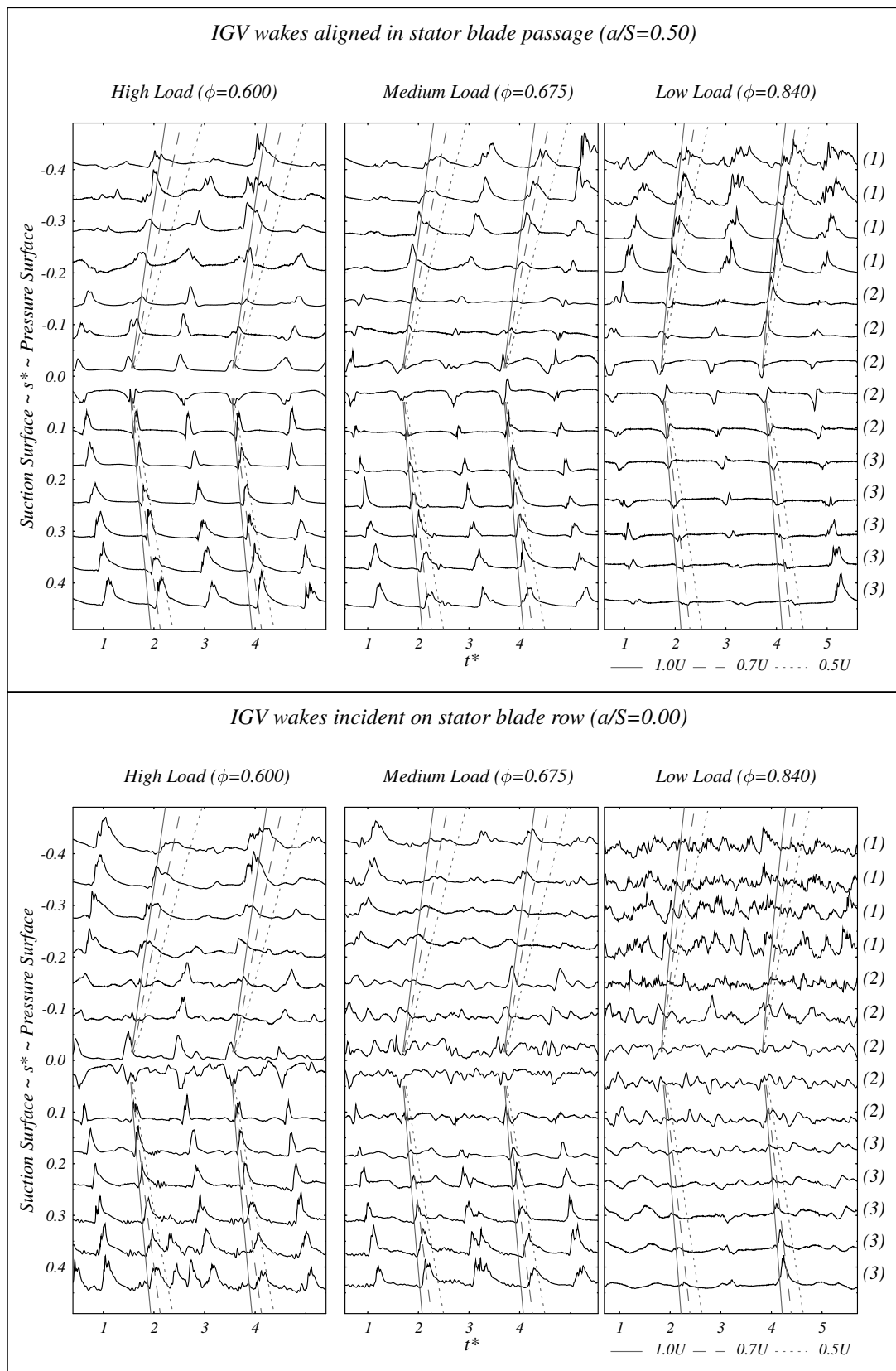


Figure 8.16: Typical raw quasi wall shear stress traces on C4 stator surface (SAG configuration). Top: IGV wakes aligned in stator passage (Case C). Bottom: IGV wakes incident on stator blade row (Case D). SAG, $Re_c = 120000$.

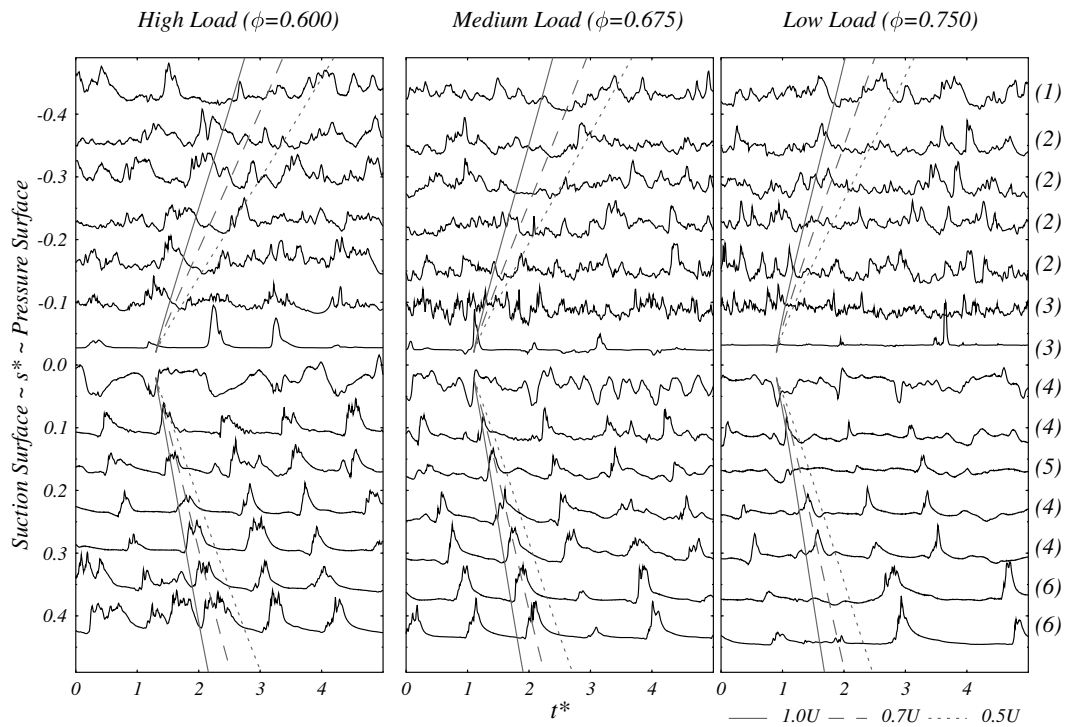


Figure 8.17: Typical raw quasi wall shear stress traces on CD stator surface (Case E, SAG, $Re_c = 120000$)

8.4 Discussion

The raw film data in Figures 8.15–8.17 and the ensemble-averaged intermittency plots in Figures 8.10–8.14 show that turbulent breakdown on the stator suction surface lags the rotor wake passage in the free-stream. Hence the simplistic engineering model of bypass transition occurring instantaneously in response to free-stream disturbances cannot apply. Boundary layer transition requires a finite interval of time and distance to complete. It commences with a region of receptivity to external disturbances that is followed by internal amplification and the appearance of secondary instabilities leading eventually to high frequency fluctuations characteristic of a turbulent spot. Figures 8.10–8.14 clearly show the wake-induced turbulent strips on the stator suction surface generally lie between particle trajectories of $0.5U$ and $0.7U$ originating at the stator leading edge. This strongly suggests that the region close to the leading edge is the most significant receptivity site in this case.

The main factors contributing to the importance of the leading edge region as the most significant receptivity site on the suction surface of a compressor blade are:

- a) the negative jet effect, which convects turbulent wake fluid away from the suction

- surface as the wake moves downstream of the leading edge;
- b) the destabilising effect of the upstream blade wake convecting over the blade leading edge;
 - c) the decelerating free-stream flow, which promotes disturbance amplification within the boundary layer.

The flow behaviour on the pressure surface of both stator blades is characteristically different from the suction surface. On the pressure surface, the negative jet causes a discharge of rotor wake fluid onto the blade surface. Perturbations from the wake jet, convecting at about $0.8 - 1.0U$, are clearly evident for the low free-stream turbulence case ($a/S = 0.5$) shown in Figs 8.15 and 8.16. At high and medium load, transition on the C4 stator does not generally commence until around $s^* = -0.5$, probably due to the boundary layer Reynolds number being too low to sustain turbulent flow ($Re_\theta \approx 180$ at $s^* = -0.5$). However, a couple of isolated turbulent breakdown events around $s^* = -0.4$ can be seen in these cases. In the low load case, the large negative incidence produces sufficient destabilisation for transition to occur close to the leading edge in the wake path. Outside the wake path, the flow separates due to the high adverse pressure gradient and a turbulent reattachment is observed to develop around $s^* = -0.3$. Transition on the pressure surface of the CD stator occurs continuously via a small leading edge separation bubble, with reattached flow detected at about $s^* = -0.05$.

Hot-film traces on both C4 and CD stator suction surfaces are much more confused in the high turbulence Cases B, D and E ($a/S = 0.0$). These observations generally show low frequency fluctuations characteristic of damped turbulent disturbances from the free-stream. The wake-induced flow features observed in the low turbulence case on the C4 stator are still evident. Increased free-stream turbulence shortens the pressure surface leading edge separation bubble on the C4 stator and causes almost continuous turbulent reattachment around $s^* = -0.1$.

Wake-induced transition phenomena on turbine blades are likely to differ from compressor blade behaviour in several respects. The boundary layer perturbations produced by wake chopping will be stabilising on the suction surface due to the opposite direction of the negative jet. The negative jet will convect fluid toward the suction surface, rather than the pressure surface, as in compressor blading. The higher blade loadings in a turbine and the resulting increased distortion (bowing) of the wake in

the blade passage, will cause the turbulent wake fluid to be in contact with a relatively larger region of the surface on a turbine blade. The flow on turbine blade is generally more stable due to the strongly accelerating free-stream flow. This makes the appearance of turbulent flow arising from leading edge unsteadiness less likely; turbulent patches near the leading edge, if they occur, may be subsequently relaminarised by the strong flow acceleration. The principal receptivity site on a turbine blade suction surface is likely to be near the pressure minimum, which will be remote from leading edge perturbations. Dovgal and Kozlov [33] reached a similar conclusion in respect of transition on an aerofoil suction surface resulting from acoustic excitation.

8.5 Conclusions

This chapter has studied unsteady flow at the leading edge of the C4 and CD stator blades. Solutions from the quasi three-dimensional flow solver, UNSFLO, were validated with experimental results from hot-film sensors. The numerical solutions were then used to interpret complex shear stress perturbations observed in the hot-film data.

Rotor wake chopping was found to have a destabilising effect on the suction surface boundary layer and a stabilising effect on the pressure surface boundary layer. This led to transition closer to the leading edge on the suction surface than would have occurred under steady flow conditions. The strength of this phenomenon was influenced by the rotor–stator axial gap, the variability of individual rotor wake disturbances, and the time-mean blade surface pressure distribution.

A variety of transition phenomena was observed at the leading edge under the rotor wake path. Wave packets characteristic of T–S wave packets were observed to amplify and break down into turbulent spots. Disturbances characteristic of the streaky structures occurring in bypass transition were also seen. Examination of suction surface disturbance and wake-induced transitional strip trajectories points to the leading edge as the principal receptivity site for suction surface transition phenomena at design loading conditions.

Different flow behaviour was observed on the pressure surface of the C4 stator, where transition occurs remote from leading edge flow perturbations caused by rotor wake chopping. The relative convection of rotor wake fluid towards the pressure surface causes the boundary layer to be more strongly influenced by passing wake

disturbances.

Decreasing the rotor–stator axial gap was observed to increase the magnitude of leading edge flow perturbations associated with wake chopping. This effect was relatively minor in comparison with the variability of wake velocity defect due to large-scale turbulent motion.

Wake chopping is expected to have less effect on unsteady wake-induced transition on the suction surface of turbine blades, where strong acceleration has a stabilising effect on the boundary layer. This moves transition further rearward along the surface, and may relaminarise incipient turbulent spots generated at the leading edge. The principal receptivity site for free-stream disturbances on a turbine blade suction surface is therefore expected to lie around the location of minimum pressure rather than the leading edge.